Epigenetic regulation of mouse sex determination by the histone demethylase Jmjd1a.

AUTHOR(S):

Kuroki, Shunsuke; Matoba, Shogo; Akiyoshi, Mika; Matsumura, Yasuko; Miyachi, Hitoshi; Mise, Nathan; Abe, Kuniya; ... Kanai, Yoshiakira; Shinkai, Yoichi; Tachibana, Makoto

CITATION:

Kuroki, Shunsuke ...[et al]. Epigenetic regulation of mouse sex determination by the histone demethylase Jmjd1a.. Science 2013, 341(6150): 1106-1109

ISSUE DATE:

2013-09-06

URL:

http://hdl.handle.net/2433/178700

Epigenetic regulation of mouse sex determination by the histone demethylase Jmjd1a

Shunsuke Kuroki[1], Shogo Matoba[2], Mika Akiyoshi[1], Yasuko Matsumura[1], Hitoshi Miyachi[1], Nathan Mise[2,8], Kuniya Abe[2], Atsuo Ogura[2], Dagmar Wilhelm[3,9], Peter Koopman[3], Masami Nozaki[4], Yoshiakira Kanai[5],Yoichi Shinkai[6*], Makoto Tachibana[1,7*]

[1]*Experimental Research Center for Infectious Diseases, Institute for Virus Research, and*

[7]*Graduate School of Biostudies, Kyoto University, 53 Shogoin, Kawara-cho, Sakyo-ku, Kyoto, Japan;*

[2]*Bioresource Center, RIKEN Tsukuba Institute, 3-1-1 Koyadai, Tsukuba, Japan;*

[3]*Institute for Molecular Bioscience, The University of Queensland, Brisbane, Queensland 4072, Australia;*

[4]*Research Institute for Microbial Diseases, Osaka University, Suita, Osaka 565-0871, Japan;*

[5]*Department of Veterinary Anatomy, The University of Tokyo, Yayoi 1-1-1, Bunkyoku, Tokyo 113-8657, Japan;*

[6]*Cellular Memory laboratory, RIKEN Advanced Science Institute, 2-1 Hirosawa, Wako-shi, Saitama 351-0198, Japan*

[8]*Present address: Department of Environmental Preventive Medicine, Jichi Medical University, 3311-1, Yakushiji, Shimotsuke, Tochigi, Japan*

[9]*Present address: Department of Anatomy and Developmental Biology, Monash University, Clayton, VIC 3800, Australia*

To whom correspondence should be addressed.

E-mail:yshinkai@riken.jp (Y.S.);mtachiba@virus.kyoto-u.ac.jp (M.T.)

ABSTRACT

Developmental gene expression is defined through cross-talk between the function of transcription factors and epigenetic status, including histone modification. Although several transcription factors play crucial roles in mammalian sex determination, how epigenetic regulation contributes to this process remains unknown. We observed male-to-female sex reversal in mice lacking the H3K9 demethylase Jmjd1a, and found that Jmjd1a regulates expression of the mammalian Y chromosome sex-determining gene *Sry*. Jmjd1a directly and positively controls *Sry* expression by regulating H3K9me2 marks. These studies reveal a pivotal role of histone demethylation in mammalian sex determination.

The development of two sexes is essential for the survival and evolution of most animal species. Although several transcription factors, including the factor encoded by the Y chromosome gene *Sry* (*1, 2*), have been shown to play crucial roles in mammalian sex differentiation, the contribution of epigenetic regulation to this process is largely unknown. *Sry* is required for male development (*3*), with sufficient and temporally accurate expression being critical for triggering the testis determining pathway (*4, 5*).

Post-translational modifications of histones are correlated with various chromatin functions, including control of gene expression. Among them, methylation of lysine 9 and lysine 4 of histone H3 (H3K9 and H3K4) are hallmarks of transcriptionally suppressed and activated chromatin, respectively (*6*). Jmjd1a (also called Tsga/Jhdm2a/Kdm3a), an enzyme that demethylates H3K9, is crucial for gene activation in spermiogenesis and metabolism (*7-12*).

When analyzing *Jmjd1a*-deficient (*Jmjd1a*Δ/Δ) mice, which had been established from [C57BL/6 (B6) x CBA] F1 ES cells (*11*), we found that XY animals were frequently sex reversed (Table S1), either partially (12 of 58 animals) with a testis and an ovary (Fig. 1A), or completely (34 of 58 animals) with two ovaries (Fig. S1). In contrast, all XY *Jmjd1a*+/+ and XY *Jmjd1a*Δ/+ mice had two testes (Fig. 1B and Table S1). Notably, some of the completely sex reversed animals were fertile (Tables S1 and S2). The generation and comparison of XY *Jmjd1a*-deficient mice, carrying the Y chromosome from either CBA (Y^{CBA}) or B6 (Y^{B6}) on a

B6 autosomal background (Fig. S2), revealed that the sex reversal phenotype was dependent on not only the loss of *Jmjd1a* but also the genetic origin of the Y chromosome combined with the B6 background. In total, 88% of XY^{CBA} but only 14% of XY^{B6} *Jmjd1a*-deficient mice displayed abnormal sex differentiation (Fig. 1B). Spermiogenesis defects were observed in XY^{CBA} as well as XY^{B6} *Jmjd1a*-deficient testes (Fig. S1), as demonstrated previously (*9, 12*). XX *Jmjd1a*-deficient mice underwent normal sex differentiation and were fertile (Table S1).

To investigate the etiology of sex reversal, we examined expression of the testicular Sertoli cell marker Sox9 (*13*) and the ovarian somatic cell marker Foxl2 (*14*) in fetal gonads after sex determination at E13.5 (Fig. 1C). XY *Jmjd1a*–deficient gonads contained both Sox9- and Foxl2-positive cells (Fig. 1D), indicative of ovotestes and therefore partial primary sex reversal, resulting from early failure of the testis-determining pathway. The number of Sox9-positive cells in XY^{B6} *Jmjd1a*-deficient gonads was significantly higher than that in XY^{CBA}. This phenotypic difference was sustained even after the 9^{th} generation of backcrossing to B6 (Fig. S3).

To address the molecular basis of this phenotype, we determined the expression levels of *Sry* and its downstream target gene, *Sox9*. A quantitative RT-PCR analysis revealed that the *Sry* expression levels were reduced to approximately 30% in XY *Jmjd1a*-deficient gonads at E11.5 [corresponding to 17-19 tail somite (ts) stages; Fig. 2A]. Expression of *Sry* was

significantly lower in XY^{CBA}, as compared to XY^{B6}, in control and mutant gonads. It is conceivable that the *Sry* expression levels in *Jmjd1a*-deficient gonads at E11.5 might be near the threshold level for inducing the male pathway, and therefore the genetic background-dependent difference of *Sry* expression may critically affect the subsequent sexual development. *Sox9* expression was also reduced in XY *Jmjd1a*-deficient gonads (Fig. 2B).

A co-immunofluorescence analysis demonstrated that the number of Sry- and Sox9-positive cells was reduced to approximately 25% in XY *Jmjd1a*-deficient gonads at E11.5 (Fig. 2, C to F). The number of Sry-positive cells in XY^{CBA} gonads was slightly, but significantly lower than that of XY^{B6} gonads at E11.5 (Fig. S4), presumably due to the different *Sry* mRNA amounts between them. On the other hand, the number of cells expressing Nr5a1, an orphan nuclear receptor expressed in gonadal somatic cells (*15*), was unchanged by *Jmjd1a* deficiency (Fig. S5). A TUNEL assay and anti-Ki67 immunostaining analysis demonstrated that *Jmjd1a* deficiency led to neither an increase in apoptosis nor a decrease in proliferation (Fig. S6). In addition, we established a transgenic mouse line (LN#9), in which the gonadal somatic cells were specifically tagged with the cell surface marker protein CD271. The gonadal somatic cells were immunomagnetically isolated from these mice with high efficiency (Fig. S7). Using these mice, we determined the numbers of gonadal somatic cells, and found that control and mutant embryos contained similar numbers at E11.5

(~4 x 10^4 cells per gonad pair, Fig. S8), indicating that *Jmjd1a* deficiency did not affect gonadal somatic cell numbers. Thus, the critical role of Jmjd1a during mammalian sex determination is to ensure *Sry* expression above the threshold level.

To identify the critical step in the male sex-determining pathway that is controlled by Jmjd1a, we used two different approaches. First, we performed a microarray analysis to address whether *Jmjd1a* deficiency results in perturbed expression of known genes required for *Sry* expression. The analysis of a total of 41,181 probes revealed 131 genes, including *Sry*, with reduced (< 0.5-fold) expression in XY *Jmjd1a*Δ/Δ, as compared to XY *Jmjd1a*Δ/+ (Table S3). However, *Jmjd1a* deficiency did not compromise expression of known *Sry* regulators (Fig. S9), indicating that Jmjd1a contributes to a different mode of *Sry* regulation. Secondly, we attempted to rescue the mutant phenotype by experimentally restoring *Sry* function, by crossing the *Hsp-Sry* transgenic mouse line (*16*) into the *Jmjd1a*-deficient background. Forced expression of *Hsp-Sry* transgene rescued the defect of testis cord development in XY *Jmjd1a*-deficient gonads to the similar levels of those of XY control gonads (Fig. S10). Furthermore, virtually no Foxl2-positive cells were observed in XY *Jmjd1a*–deficient gonads expressing the *Hsp-Sry* transgene (Fig. S10), indicating that *Sry* acts epistatically to *Jmjd1a* in regulating male sex determination in mice.

We next investigated the expression profile of Jmjd1a protein during gonadal development. Jmjd1a was detected in gonadal somatic and germ cells, but not in mesonephric

cells at E11.5 (18ts) (Fig. 3A). A comparative RT-qPCR analysis revealed that *Jmjd1a* was the most highly transcribed gene in E11.5 gonadal somatic cells, among those encoding enzymes involved in the maintenance of H3K9 methylation (Fig. S11). An RNA expression analysis indicated that the amount of *Jmjd1a* mRNA increased from E10.5 (8 to 10ts) and reached a plateau around E11.5 in gonadal somatic cells (Fig. 3B). This temporal expression profile is consistent with direct regulation of *Sry* expression by Jmjd1a. An immunofluorescence analysis demonstrated that *Jmjd1a* deficiency resulted in an approximately two-fold increase in the signal intensities of H3K9me2 in gonadal cells at E11.5 (Fig. 3C and D), indicating its substantial contribution to H3K9 demethylation. *Sry* expression is triggered in the center of XY gonads at around 12ts (*17, 18*). We observed low levels of H3K9me2 throughout XY gonads at 12ts (Figure S12), suggesting that Jmjd1a demethylates H3K9me2 prior to *Sry* expression. Abundant Jmjd1a expression and low levels of H3K9me2 were also observed in XX gonads at E11.5 (Figure S13).

To prove the direct link between Jmjd1a function and *Sry* expression, a chromatin immunoprecipitation (ChIP) analysis was performed, using purified gonadal somatic cells at E11.5. Jmjd1a was bound to regulatory regions within the *Sry* locus in wild type cells (Fig. 4A and B). *Jmjd1a* deficiency led to a significant increase in H3K9me2 levels within the *Sry* locus (Fig. 4C), without changing histone H3 occupancy (Fig. 4D). The H3K9me2 levels of the *Sry* locus were indistinguishable between XY^{B6} and XY^{CBA} gonads at E11.5 (Fig. S14),

demonstrating the conserved role of Jmjd1a between these genetic backgrounds. The unchanged levels of H3K9me3 at the *Sry* locus, with or without Jmjd1a, indicated H3K9me2-specific demethylation by Jmjd1a (Fig. 4E). *Jmjd1a* deficiency resulted in perturbed H3K4 methylation of the *Sry* locus (Fig. 4F). In contrast to *Sry*, the H3K9me2 levels of *Sox9* were unchanged by *Jmjd1a* deficiency (Fig. S15), indicating that Jmjd1a does not control *Sox9* expression directly. Coordinated H3K9 demethylation/H3K4 methylation was commonly observed in other Jmjd1a target genes (Fig. S15), suggesting that Jmjd1a-mediated H3K9 demethylation is required for subsequent H3K4 methylation for transcriptional activation. Since *Sry* is located on the heterochromatic Y chromosome, Jmjd1a-mediated H3K9 demethylation may induce de-heterochromatinization of *Sry,* to allow the access of the H3K4 methyltransferase and transcription factors (Fig. S16).

This work shows a crucial role of a histone demethylase in *Sry* expression. Another chromatin regulator, Cbx2, reportedly plays a role in *Sry* expression in mice (*19*). However, in contrast to Jmjd1a, Cbx2 up-regulates the expression of several positive regulators of *Sry*, such as *Dax1*, *Gata4*, *Wt1* and *Nr5a1* (*19*), suggesting that they might be involved in different phases of *Sry* expression. The discovery of the critical role of chromatin modification on *Sry* regulation not only provides new insights into the earliest steps of mammalian sex determination, but also demonstrates the importance of epigenetic regulation in spatio-temporal gene regulation during embryonic development.

FIGURE LEGENDS

Figure 1. *Jmjd1a*-deficient mice show XY sex reversal

(A) Internal genitalia of partially sex reversed XY *Jmjd1a*-deficient mice. Ov, ovary; Ut, uterus; Te, testis; Ep, epididymis. **(B)** Frequency analysis of abnormal sex differentiation between XY^{CBA} and XY^{B6} mice, determined by examining internal genitalia of adult mice. Genital classification is described in Table S1 and Fig. S1. Numbers of examined animals are shown above the bars. **(C)** Immunofluorescence analysis of E13.5 gonads. Sox9 and Foxl2 mark testicular Sertoli and ovarian somatic cells, respectively. Scale bar, 100 μm. **(D)** Quantification of Sox9- and Foxl2-positive cells in E13.5 gonads. Numbers of examined embryos are shown above the bars. Data are presented as mean±s.e. $^{**}P<0.01$, $^{***}P<0.001$ (Student's *t*-test).

Figure 2. *Jmjd1a* deficiency perturbs the expression of *Sry*

(A and **B)** Quantitative RT-PCR analyses of *Sry* (A) and *Sox9* (B) in XY gonads. Each of the samples included one pair of gonads/mesonephros. Results were normalized to *Gapdh,* and the expression levels in XY^{B6} *Jmjd1a*Δ/+ were defined as 1. Numbers of examined embryos are shown above the bars. (**C** and **E)** Co-immunostaining profiles of Sry (C) and Sox9 (E) with the gonadal somatic cell marker, Gata4, in XY^{CBA} gonads. (**D** and **F**) The ratios of the

cells positive for Sry (D) and Sox9 (F) to the cells positive for Gata4. Scale bar, 50 μm. All data are presented as mean±s.e. *P<0.05, **P<0.01, ***P<0.001 (Student's t-test).

Figure 3. Jmjd1a is expressed in developing gonads and catalyzes H3K9 demethylation

(A) Co-immunostaining profiles of Gata4 and Jmjd1a on sections of XY^{CBA} gonads. Enlarged box indicates that Jmjd1a signals were observed in gonadal somatic cells as well as germ cells (asterisks). G, gonad; M, mesonephros. Scale bar, 50 μm. (**B**) Quantitative analysis of *Jmjd1a* transcripts in purified gonadal somatic cells. Expression is normalized to *Gapdh*. Numbers of examined embryos are shown above the bars. (**C**) Co-immunostaining profiles of Gata4 and H3K9me2 in XY^{CBA} gonads. G, gonad; M, mesonephros. Scale bar, 50 μm. (**D)** Quantitative comparison of the immunofluorescence intensities of H3K9me2 signals between gonadal and mesonephric cells. The intensities of H3K9me2 signals in *Jmjd1a*Δ/+ mesonephric cells were defined as 1. MC, mesonephric cells; GC, gonadal cells. All data are presented as mean±s.e. *P<0.05, **P<0.01 (Student's t-test).

Figure 4. Jmjd1a directly regulates H3K9 demethylation in the *Sry* locus.

(A) Diagram of the *Sry* locus and the location of primer sets for ChIP-qPCR. (B) Chromatin immunoprecipitation (ChIP) analysis with anti-Jmjd1a, using purified XY^{CBA} gonadal somatic cells. GSC, gonadal somatic cells; MC, mesonephric cells. (C to F), ChIP analysis for

H3K9me2 (C), pan-H3 (D), H3K9me3 (E) and H3K4me2 (F), at the *Sry* linear promoter region of purified XY^{CBA} gonadal somatic cells. All data are presented as mean±s.e. **P*<0.05, ***P*<0.01 (Student's *t*-test).

References and Notes

1. R. Sekido, R. Lovell-Badge, *Trends Genet.* **25**, 19 (2009).

2. K. Kashimada, P. Koopman, *Development* **137**, 3921 (2010).

3. P. Koopman, J. Gubbay, N. Vivian, P. Goodfellow, R. Lovell-Badge, *Nature* **351**, 117 (1991).

4. R. Hiramatsu *et al.*, *Development* **136**, 129 (2009).

5. D. Wilhelm *et al.*, *Mech. Dev.* **126**, 324 (2009).

6. S. M. Kooistra, K. Helin, *Nat. Rev. Mol. Cell. Biol.* **13**, 297 (2012).

7. K. Yamane *et al.*, *Cell* **125**, 483 (2006).

8. M. Tachibana, M. Nozaki, N. Takeda, Y. Shinkai, *EMBO J.* **26**, 3346 (2007).

9. Y. Okada, G. Scott, M. K. Ray, Y. Mishina, Y. Zhang, *Nature* **450**, 119 (2007).

10. K. Tateishi, Y. Okada, E. M. Kallin, Y. Zhang, *Nature* **458**, 757 (2009).

11. T. Inagaki *et al.*, *Genes Cells* **14**, 991 (2009).

12. Z. Liu *et al.*, *J. Biol. Chem.* **285**, 2758 (2010).

13. J. Kent, S. C. Wheatley, J. E. Andrews, A. H. Sinclair, P. Koopman, *Development* **122**, 2813 (1996).

14. K. A. Loffler, D. Zarkower, P. Koopman, *Endocrinology* **144**, 3237 (2003).

15. K. Morohashi, S. Honda, Y. Inomata, H. Handa, T. Omura, *J. Biol. Chem.* **267**, 17913

(1992).

16. T. Kidokoro *et al.*, *Dev. Biol.* **278**, 511 (2005).

17. M. Bullejos, P. Koopman, *Dev. Dyn.* **221**, 201 (2001).

18. K. H. Albrecht, E. M. Eicher, *Dev. Biol.* **240**, 92 (2001).

19. Y. Katoh-Fukui *et al.*, *Endocrinology* **153**, 913 (2012).

20. We are especially grateful to T. Nakano for critical advice during the manuscript preparation. We thank K. Morohashi for anti-Nr5a1 antibodies; H. Kimura for anti-histone antibodies; and T. Hara for FACS analysis support. We are also grateful to T. Matsui, G. Nagamatsu and the members of the Tachibana laboratory for technical support. This work was supported by grants from the Funding Program for Next Generation World-leading Researchers (M.T.). The microarray data have been deposited in Gene Expression Omnibus and given the accession number GSE49513.

Supporting Online Material

Figs. S1 to S16

Tables S1 to S4

References

Figure 1

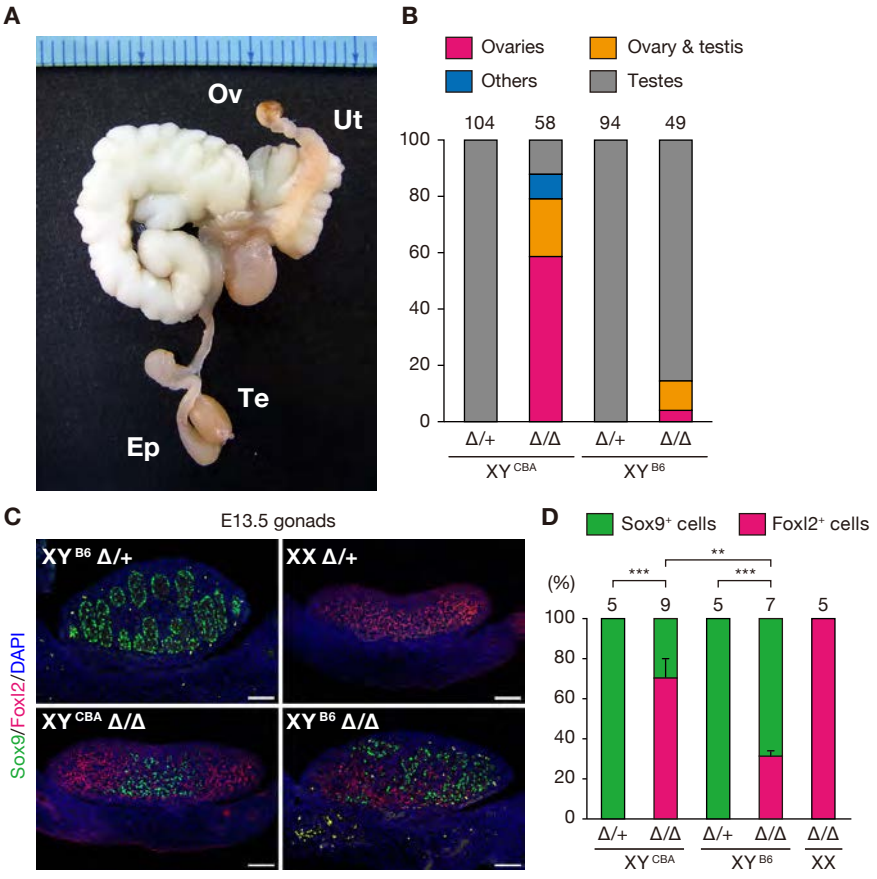

Figure 2

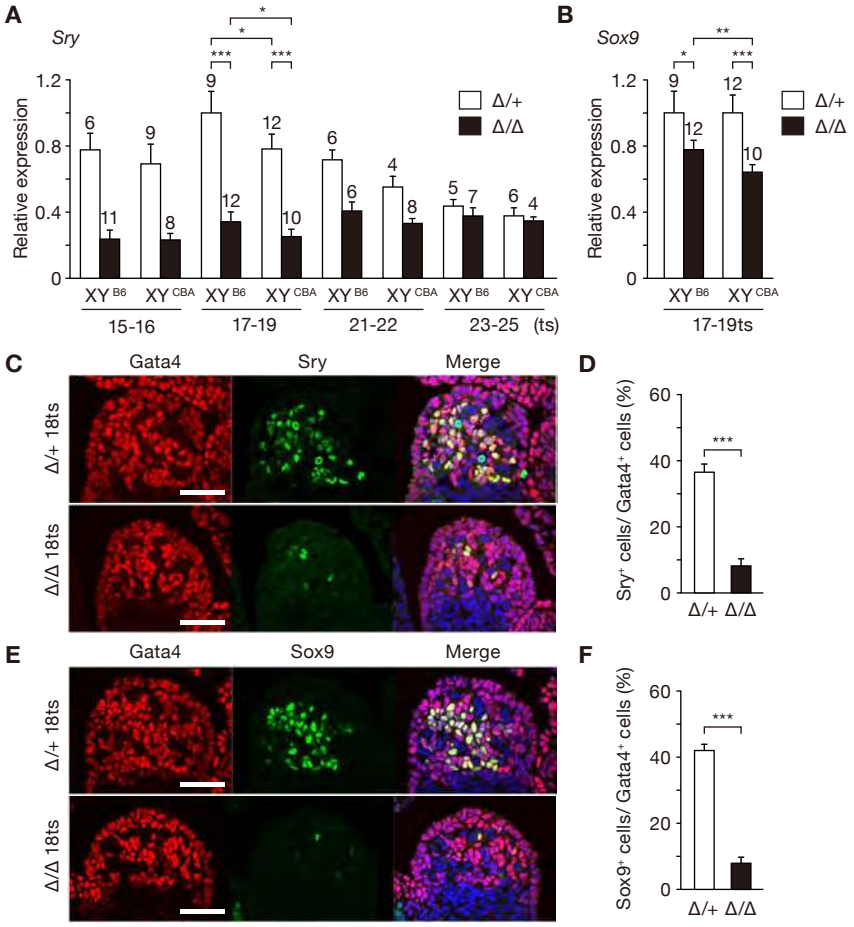

Figure 3

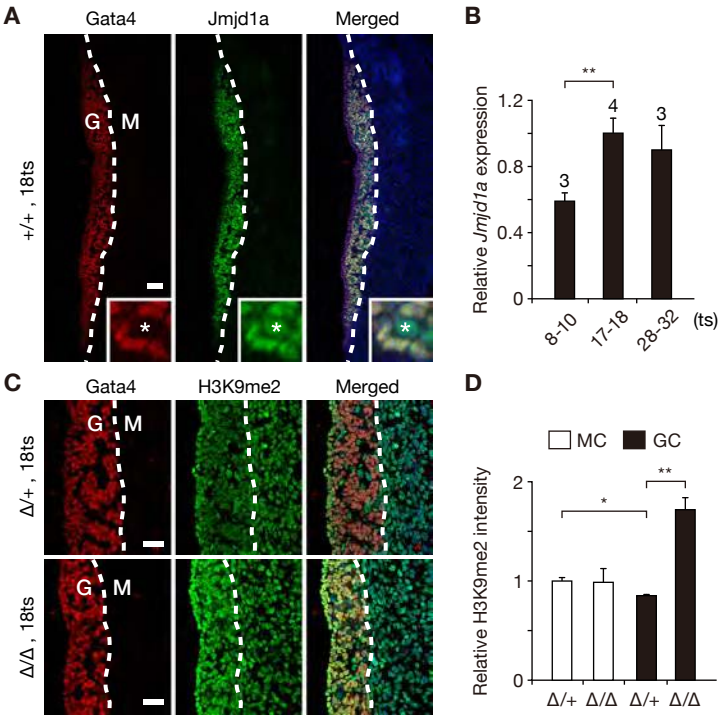

Figure 4

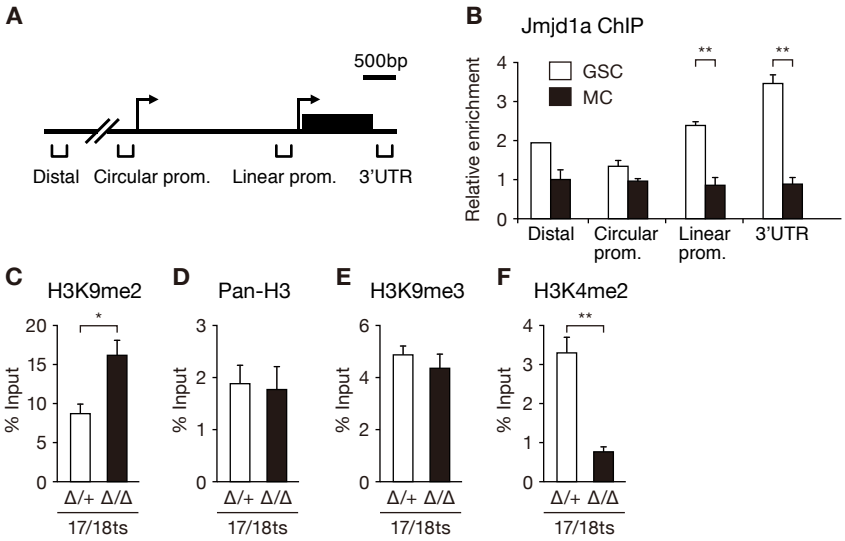

Supplementary Materials for

Epigenetic regulation of mouse sex determination by the histone demethylase Jmjd1a

Shunsuke Kuroki, Shogo Matoba, Mika Akiyoshi, Yasuko Matsumura, Hitoshi Miyachi, Nathan Mise, Kuniya Abe, Atsuo Ogura, Dagmar Wilhelm, Peter Koopman, Masami Nozaki, Yoshiakira Kanai,Yoichi Shinkai*, Makoto Tachibana*

* Corresponding author. E-mail: yshinkai@riken.jp (Y.S.); mtachiba@virus.kyoto-u.ac.jp (M.T.)

This PDF file includes:

Materials and Methods
Figs. S1 to S16
Tables S1, S2 and S4
References (*20*-*23*)

Other Suplementary Materials for this manuscript includes the following:

Table S3: List of Jmjd1a-regulated genes identified by microarray analysis (as an Excel file)

Materials and Methods

Antibodies

Rabbit polyclonal antibodies against Jmjd1a were described previously (*8*). Additional antibodies used in this study were as follows: goat anti-Gata4 (Santa Cruz), rabbit anti-Sry (*20*), rabbit anti-Sox9 (*16*), goat anti-Foxl2 (abcam), mouse anti-H3K9me2 (*21*), mouse anti-H3K9me3 (*21*), mouse anti-H3K4me2 (*21*), rat anti-pan H3 (gift from Dr. H. Kimura), rabbit anti-Ki67 (Abcam), TRA98 antibody (Bio Academia), rabbit anti-Nr5a1 (gift from Dr. K. Morohashi).

Histology and Immunochemistry

Tissues were fixed in either Bouin's solution or 4% paraformaldehyde, embedded in paraffin, and cut into 4-μm sections. For histological analysis, hematoxylin and eosin (H&E) or hematoxylin and PAS staining was performed using standard protocols. For immunohistochemistry, sections were deparaffinized and rehydrated, and autocleaved at 105℃ for 5 minutes in 10mM citric acid buffer (pH 6.0). To quench endogenous peroxidase, the sections were treated with 0.3% (v/v) hydrogen peroxide. After blocking with TBS containing 2% skim milk and 0.1% Triton-X100 at RT for 1h, sections were incubated overnight with primary antibodies at 4℃. For fluorescence staining, the sections were rinsed and incubated with Alexa-conjugated secondary antibodies at RT for 1h, and counterstained with DAPI. The sections were mounted in Vectashield (Vector) and observed with confocal laser scanning microscope (LSM700, Carl Zeiss). Mean fluorescence intensities per area were measured by ImageJ software (National Institutes of Health) at mesonephric or gonadal regions in each genotype. Fluorescence intensities of mesonephric cells in *Jmjd1a* Δ/+ were defined as 1.

Quantitative RT-PCR

Total RNA was purified using RNeasy kit (QIAGEN). First strand DNA synthesis was performed using Super Script III (Invitrogen). SYBR Premix Ex taq II was used for qRT-PCR. Primer sequences are listed in Table S4.

Microarray analysis

RNA was collected with Trizol LS (Life technologies) from immunomagnetically purified gonadal somatic cells from a pair of gonads of *Nr5a1/CD271* transgenic embryos at 18ts (fig. S7). Analyzed RNAs were as follows: XY^{CBA} *Jmjd1a* Δ/+ (n=3), XY^{CBA} *Jmjd1a* Δ/Δ (n=3), XX *Jmjd1a* Δ/+ (n=3) and XX *Jmjd1a* Δ/Δ (n=3). A low input Quick Amp Labelig kit (Agilent Technologies) was used for the linear amplification and labeling of RNAs. After assessment of the integrity of Cy3-labeled RNAs by Agilent 2100 Bioanalyzer using RNA 6000 Nano kits (Agilent Technologies), they were hybridized to Mouse Whole Genome microarray (Agilent Technologies). Microarray images were captured by DNA Microarray Scanner (Agilent Technologies). Signal intensity data were extracted from the scanned images by Feature Extraction software (Agilent Technologies) and they were analyzed with GeneSpring GX12 (Agilent Technologies).

ChIP analysis

For anti-Jmjd1a ChIP analysis, 7×10^5 undifferentiated gonadal somatic cells and equal numbers of mesonephric cells were immunomagnetically separated from twenty embryos (E11.5) expressing *Nr5a1/CD271*-transgene. Cells were then mixed with 1×10^7 of XX MEFs, crosslinked with 1% formaldehyde and applied to ChIP analysis with anti-Jmjd1a antibodies. ChIP analysis of histone modification was described previously (*22*). Briefly, gonadal somatic cells (approximately 4×10^4) were immunomagnetically purified from an E11.5 embryo. Chromatin fractions were prepared from the gonadal somatic cells, digested with micrococcal nuclease, and then applied to ChIP analysis using anti-modified histone antibodies. Primer sequences are listed in Table S4.

Flow cytometry

Cells stained with anti CD271-FITC (Milteny Biotec) and propidium iodide were analyzed with a FACSCalibur flow cytometer (BD). Data on 10,000 viable cells were collected for each sample and analyzed with CellQuest software (BD).

Mice

All animal experiments were performed under the animal ethical guidelines of Kyoto University. Generation of mice *Jmjd1a*-deficient mice and mice carrying *Sry* transgene of from mouse strain 129 with *Hsp* promoter were described previously (*11, 16*).

Establishment of *Nr5a1/CD271*-transgenic mice

The detailed strategy for the establishment of *Nr5a1/CD271*-transgenic mice is presented in fig. S7. Briefly, a BAC clone containing all exons of *Nr5a1* was modified by replacing *Nr5a1* initiation codon with the sequences for *hCD271* and polyA signals, and was then introduced into fertilized eggs of C57BL/6J. We obtained three independent transgenic mice lines carrying the *Nr5a1/CD271*-transgene (LN#1, LN#9 and LN#12). From these, we used LN#9 in this study. All animal experiments were performed under the animal ethical guidelines of Kyoto University.

Isolation of gonadal somatic cells

A scheme for the purification of gonadal somatic cells is illustrated in fig. S7. Briefly, single cell suspension was prepared by trypsinizing gonads and mesonephroi isolated from embryos carrying the *Nr5a1/CD271*-transgene. Immunomagnetic isolation of CD271-expressing cells was performed according to the standard protocols (Miltenyi Biotech).

TUNEL assay

The TUNEL assay was performed following the manufacturer's instruction (Roche).

Figure S1. Kuroki et al.

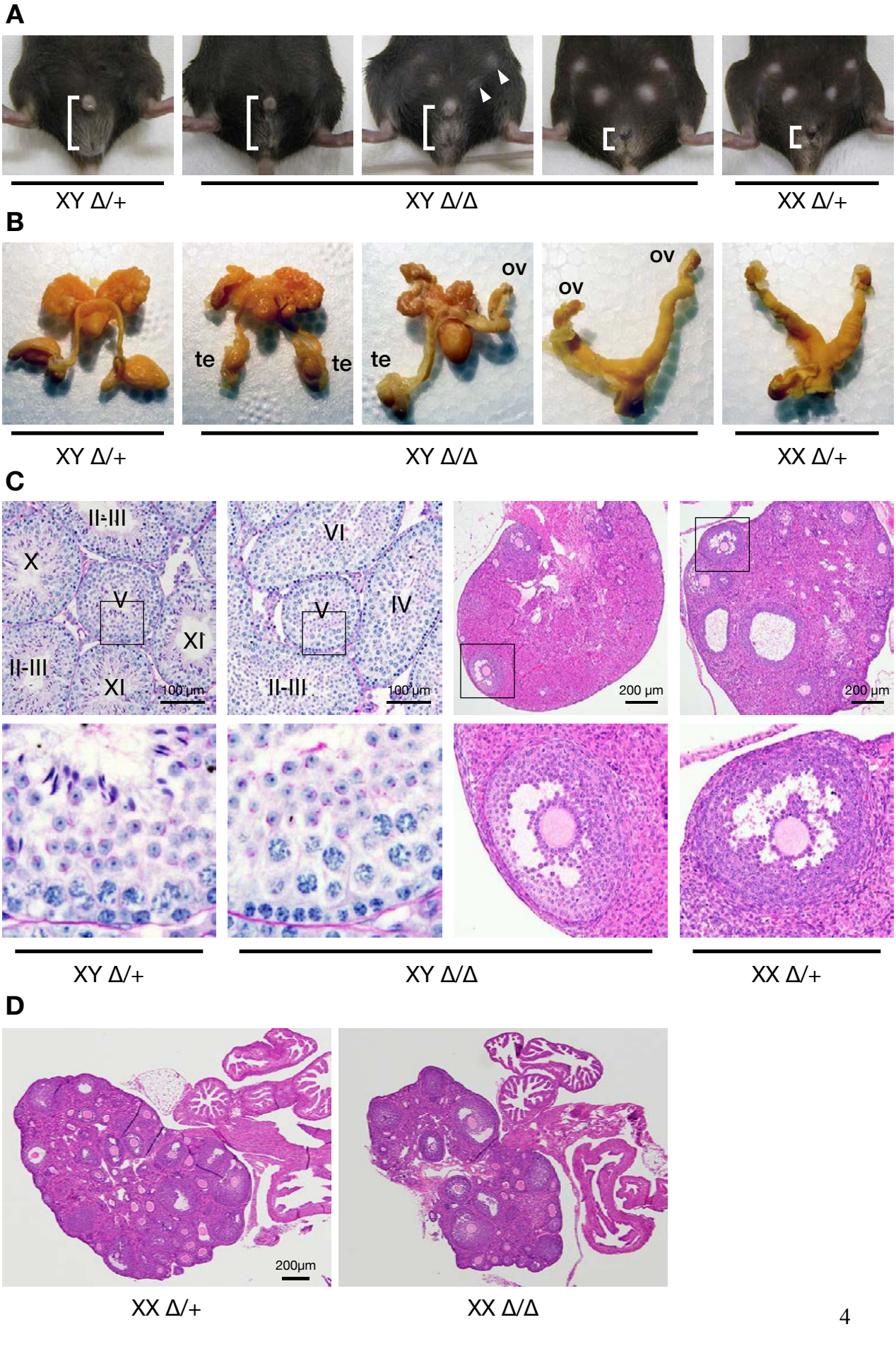

Fig. S1. Analysis of sexual development of XY^{CBA} *Jmjd1a*-deficient adult mice.

(**A**) External genitalia of adult mice of indicated genotypes. The distance between anus and penis or vagina is indicated. Arrowheads represent mammary glands. (**B**) Gonads and genital tracts of adult mice of indicated genotypes. te, testis; ov, ovary. (**C**) Cross-section of testes (left two panels) and ovaries (right two panels) of indicated genotypes. Roman numerals refer to the stages of mouse spermatogenesis. Areas in boxes are shown at higher magnification. Stage V of the cycle of seminiferous epithelium of *Jmjd1a*-deficient testis lacks elongating spermatids. (**D**) HE-stained cross-section of ovaries (2-month old) of indicated genotypes . Growing oocytes were abundant in XX *Jmjd1a*-deficinet ovary (right) as well as that of control (left).

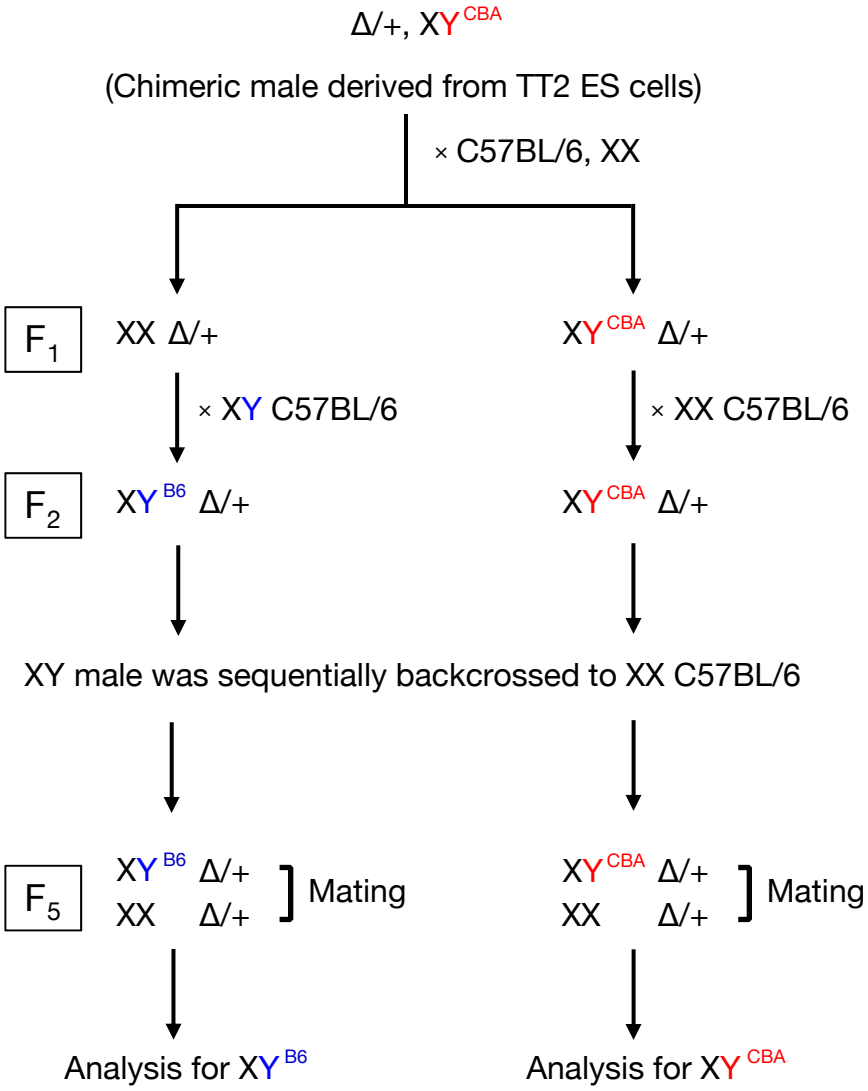

Fig. S2. Strategy for generation of *Jmjd1a* deficient mice with different Y chromosomes.

Jmjd1a Δ/+ chimeric male was generated using TT2 ES cells, which was established form a F1 blastocyst between a C57BL/6 female and a CBA male (*23*). Chimeric male and F1 female were sequentially crossed to C57BL/6 and F_5 generation were analyzed.

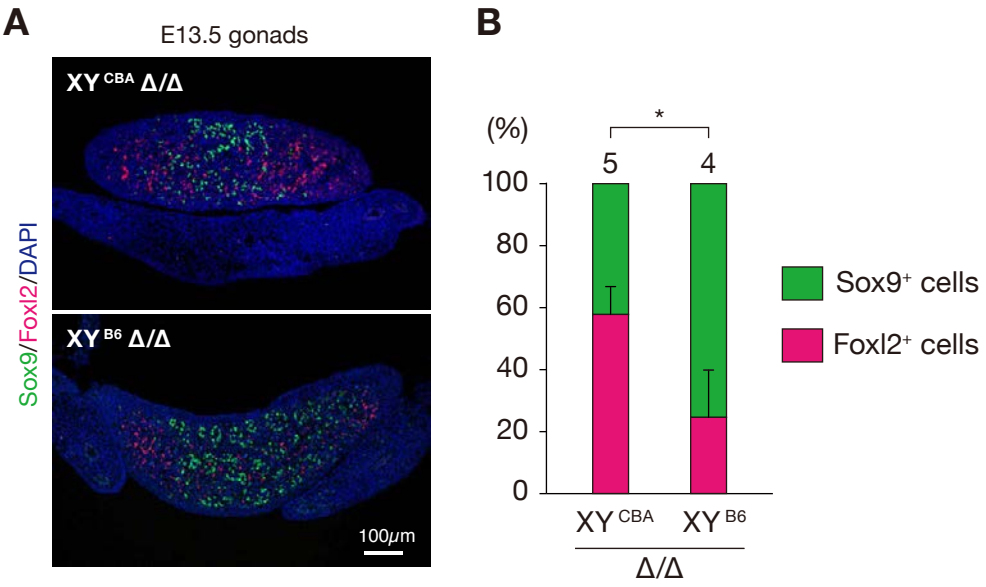

Fig. S3. Immunofluorescence analysis of E13.5 gonads of the mice at the 9th generation of backcrossing to B6.

XY *Jmjd1a* Δ/+ mice carrying either Y^{B6} or Y^{CBA} were sequentially backcrossed to C57BL/6 and sexual development of F_9 generation was analyzed. (**A**) Co-immunostaining profiles of Sox9 and Foxl2 in XY gonads of the indicated stage and genotypes. (**B**) Quantification of Sox9- and Foxl2-positive cells in E13.5 gonads of indicated genotypes. Numbers of examined embryos are shown on top. Data are presented as mean±s.e. **P*<0.05 (Student's *t*-test).

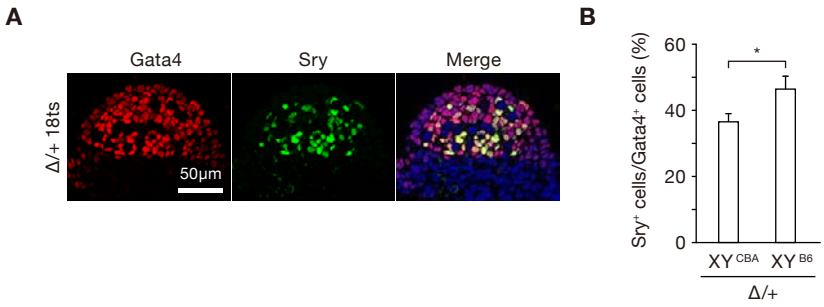

Fig. S4. Comparison of Sry expression in E11.5 gonads between XY^{B6} and XY^{CBA}. (**A**) Co-immunostaining profiles of Sry with the gonadal somatic cell marker, Gata4 in XY^{B6} gonads of the indicated stage and genotype. (**B**) Comparison of the ratio of the cells positive for Sry to the cells positive for Gata4 of indicated XY gonads at E11.5. Data are presented as mean±s.e. **P*<0.05 (Student's *t*-test).

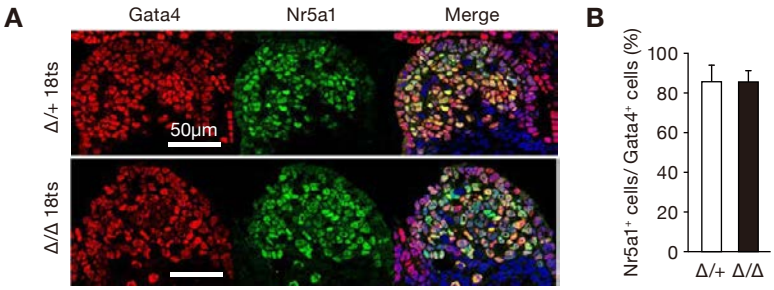

Fig. S5. *Jmjd1a*-deficiency does not affect Nr5a1 expression.

(**A**) Co-immunostaining profiles of Nr5a1with the gonadal somatic cell marker, Gata4 in XY^{CBA} gonads of the indicated stage and genotypes. (**B**) The ratio of the cells positive for Nr5a1 to the cells positive for Gata4. Data are presented as mean±s.e.

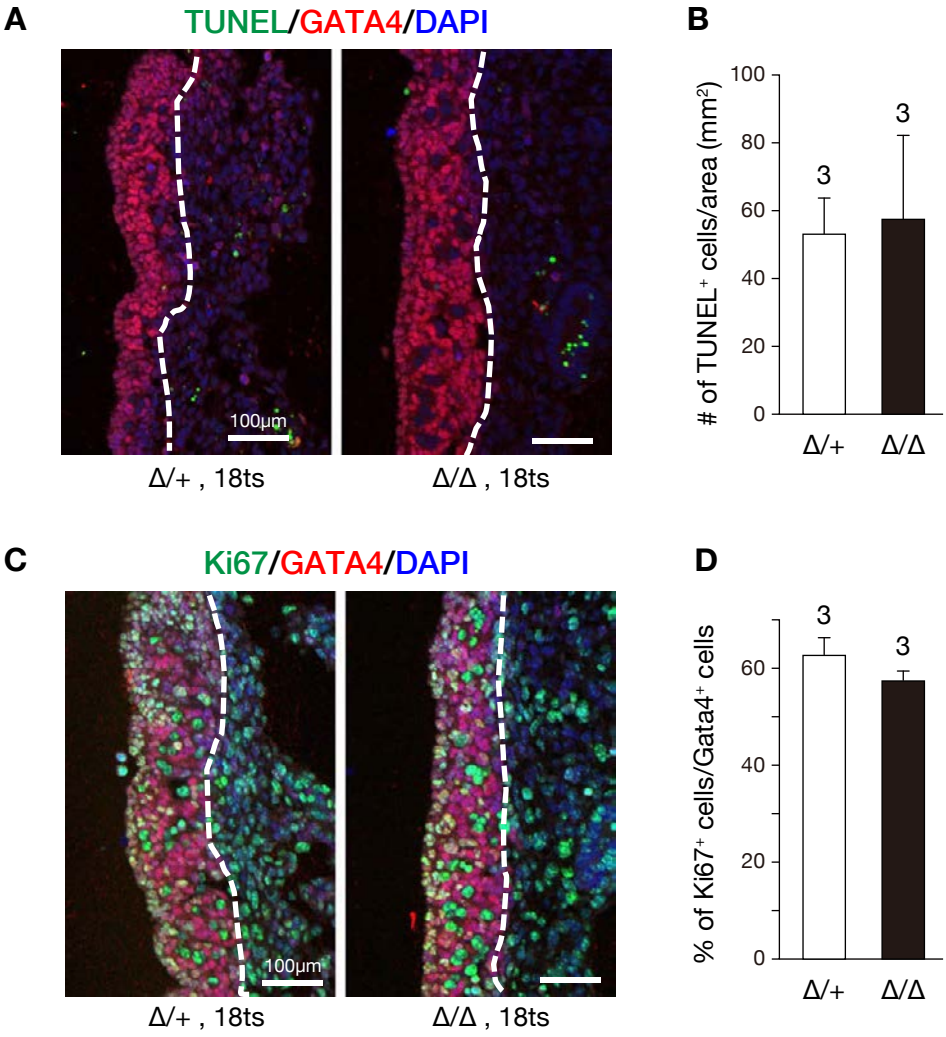

Fig. S6. Apoptosis and proliferation analysis of XY^{CBA} gonads at E11.5.

(**A**) TUNEL-stained section of XY^{CBA} gonads of the indicated stage and genotypes were counterstained with anti-Gata4 antibodies. (**B**) Average numbers of gonadal apoptotic cells are summarized. (**C**) Double immunostaining analysis with anti-Ki67 and anti-Gata4 antibodies of the indicated stage and genotypes. (**D**) Average numbers of Ki67-positve cells per Gata4-positive cells are summarized. Numbers of examined embryos are represented on top. Data are presented as mean±s.e.

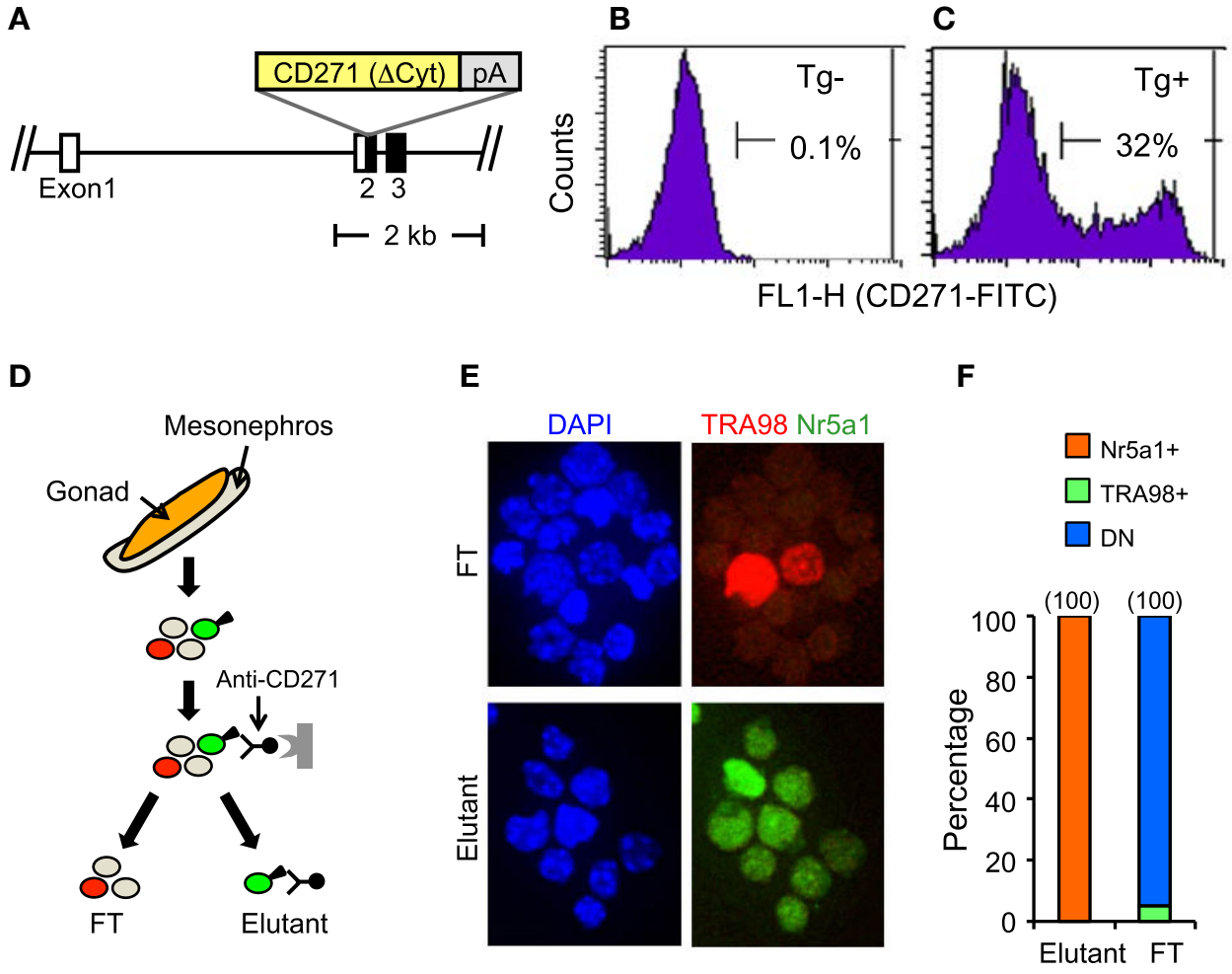

Fig. S7. Establishment of transgenic mice expressing hCD271 in *Nr5a1* promoter-dependent manner.

(**A**) Diagram of the *Nr5a1/CD271* BAC transgene. The *Nr5a1* initiation codon in a BAC (clone, RP24-102N10) containing full exons of *Nr5a1*, was replaced by the sequences for *hCD271* and polyA signals. ΔCyt represents the mutant form without the DNA sequences for cytoplasmic portion. (**B** and **C**) Flowcytometric analysis of *Nr5a1/CD271* transgenic mice. Cells were prepared from E11.5 gonads with mesonephroi of *Nr5a1/CD271* transgene-negative (Tg-) (B) and positive (Tg+) lines (C), and then stained with anti-CD271-FITC antibodies. (**D**) Schematic representation for the isolation of gonadal somatic cells. Cells are represented as follows: Green, gonadal somatic cells; Grey, other somatic cells (mainly derived from mesonephroi); Red, germ cells. FT, flow-through. (**E**) Typical immunostaining profiles of the purified cells. TRA98 antibody (red) and anti-Nr5a1 antibodies (green) were used for detection of germ cells and gonadal somatic cells, respectively. (**F**) Purity of the fractionated cells as determined by immunostaining. Numbers of examined cells are represented on top of graphs. DN, doubly negative cells for TRA98 and Nr5a1 signals.

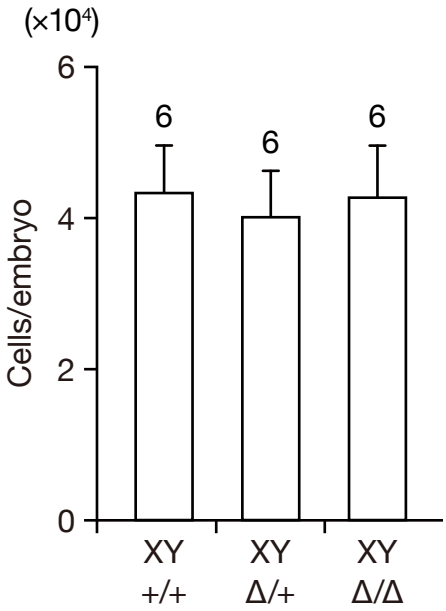

Fig. S8. Number of gonadal somatic cells in XY^{CBA} *Jmjd1a*-deficient gonads.
Gonadal somatic cells were immunomagnetically purified from E11.5 *Nr5a1/CD271*-TG embryos of indicated genotypes. Data presented are means±s.e. Numbers of examined embryos are represented on top.

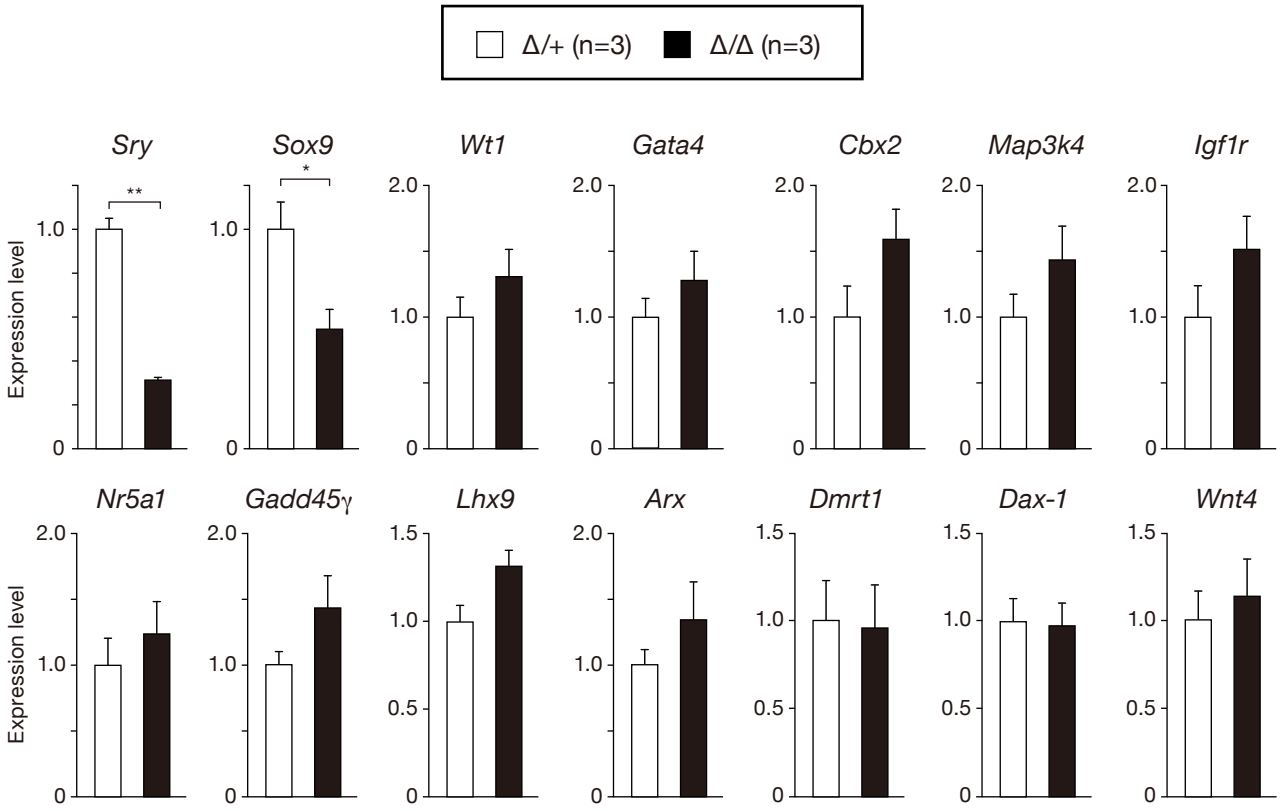

Fig. S9. Expression microarray analysis for the genes involved in sex determination and/or gonadgeneisis in E11.5 XY^{CBA} gonadal somatic cells.

RNAs were prepared from isolated gonadal somatic cells at 18ts, and then subjected to expression microarray analysis. Expression levels in XY *Jmjd1a* Δ/+ were arbitrarily set as 1. Data are presented as means±s.e. **P*<0.05, ***P*<0.01 (Student's *t*-test).

Figure S10. Kuroki et al.

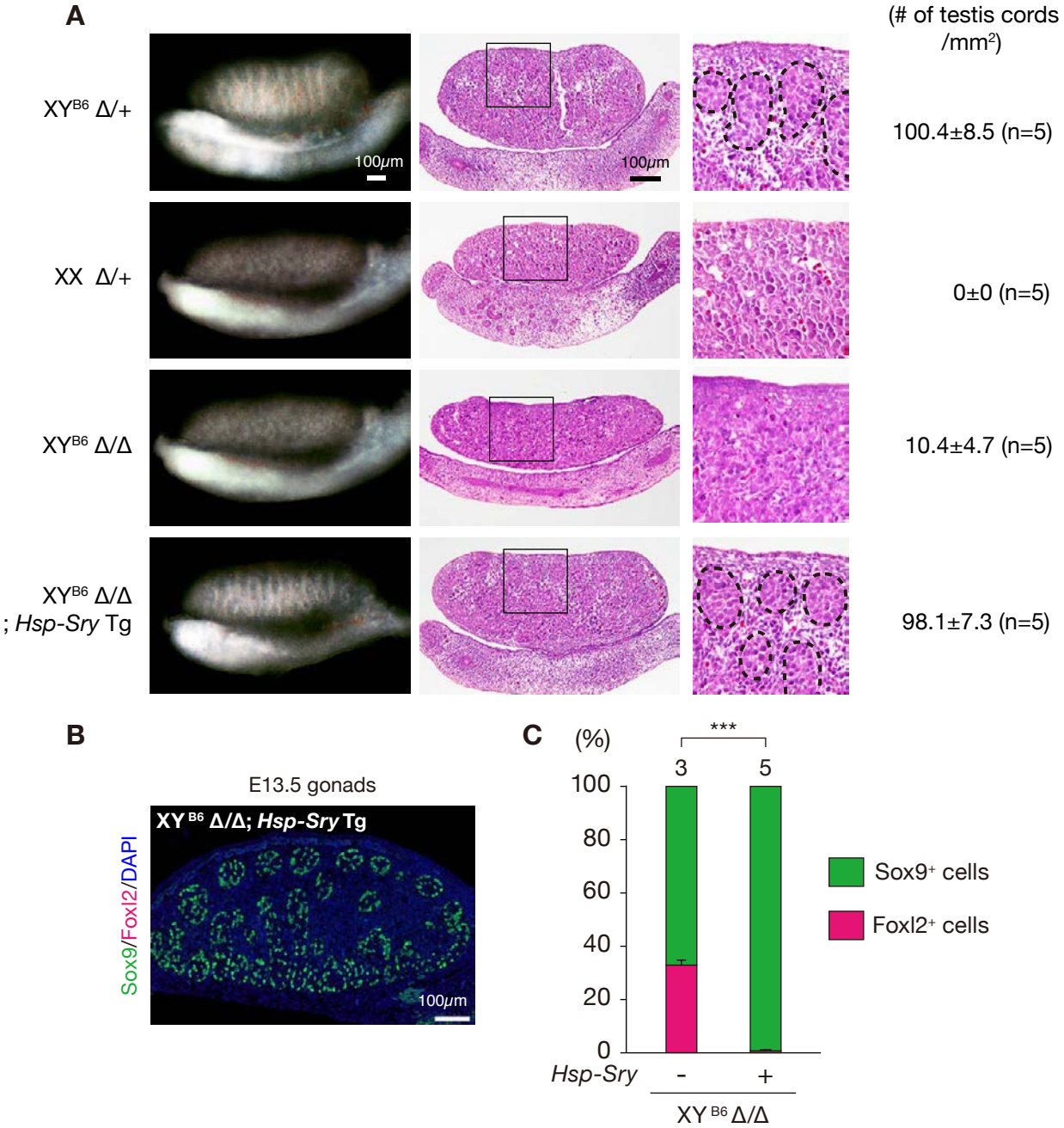

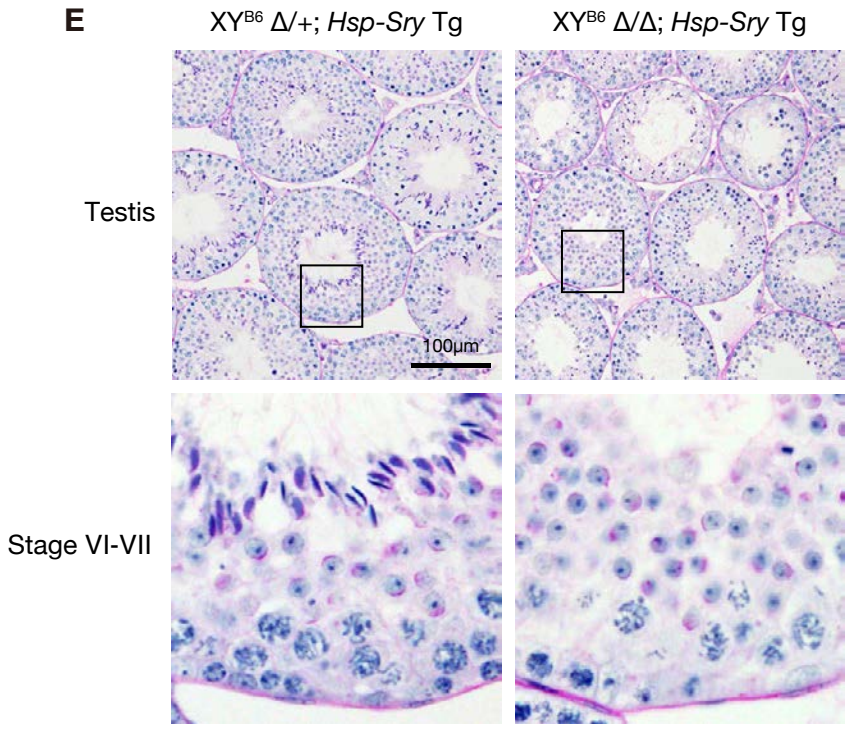

Fig. S10. Exogenous expression of *Hsp-Sry* transgene (strain 129 origin) rescues abnormal sexual development of *Jmjd1a*-deficent XY^{B6} gonads on B6 genetic background.

(**A**) Gross morphology analysis (left) and histology of HE-stained sections (Middle) of E13.5 gonads of indicated genotypes. Areas in boxes are shown at higher magnification (right). Dotted circles indicate testis cords. Number of testis cords on the sections were counted and summarized in the right. (**B**) Immunofluorescence analysis for Sox9 and Foxl2 in E13.5 gonad of XY^{B6} *Jmjd1a*-deficinet embryo carrying *Hsp-Sry* transgene. (**C**) Quantification of Sox9- and Foxl2-positive cells in E13.5 gonads of indicated genotypes. Numbers of examined embryos are shown above the bars. Data are presented as mean±s.e. ***P<0.001 (Student's t-test). (**D**) HE-stained cross-section of epididymides of 3-month-old mice of indicated genotypes. XY^{B6} *Jmjd1a*-deficent epididymides carrying *Hsp-Sry* transgene lack mature sperm. (**E**) Hematoxylin PAS-stained section of testes (3-month-old) of indicated genotypes. Areas in boxes are shown at higher magnification. Roman numerals refer to the stages of mouse spermatogenesis. Stage VI-VII of the cycle of seminiferous epithelium of XY^{B6} *Jmjd1a*-deficent testis carrying *Hsp-Sry* transgene lacks elongating spermatids.

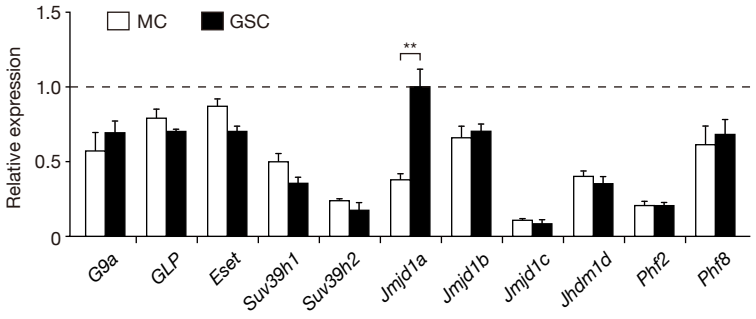

Fig. S11. Expression of mRNAs encoding enzymes that regulate H3K9 methylation in gonads of XY^{CBA} wild type embryos at E11.5.

Gonadal somatic cells (GSC) and mosonephric cells (MC) were immunomagnetically separated and then applied to RNA expression analysis. Levels were normalized to *Gapdh*. The expression levels of *Jmjd1a* in GSC were defined as 1. Data are presented as mean±s.e. $^{**}P<0.01$ (Student's *t*-test).

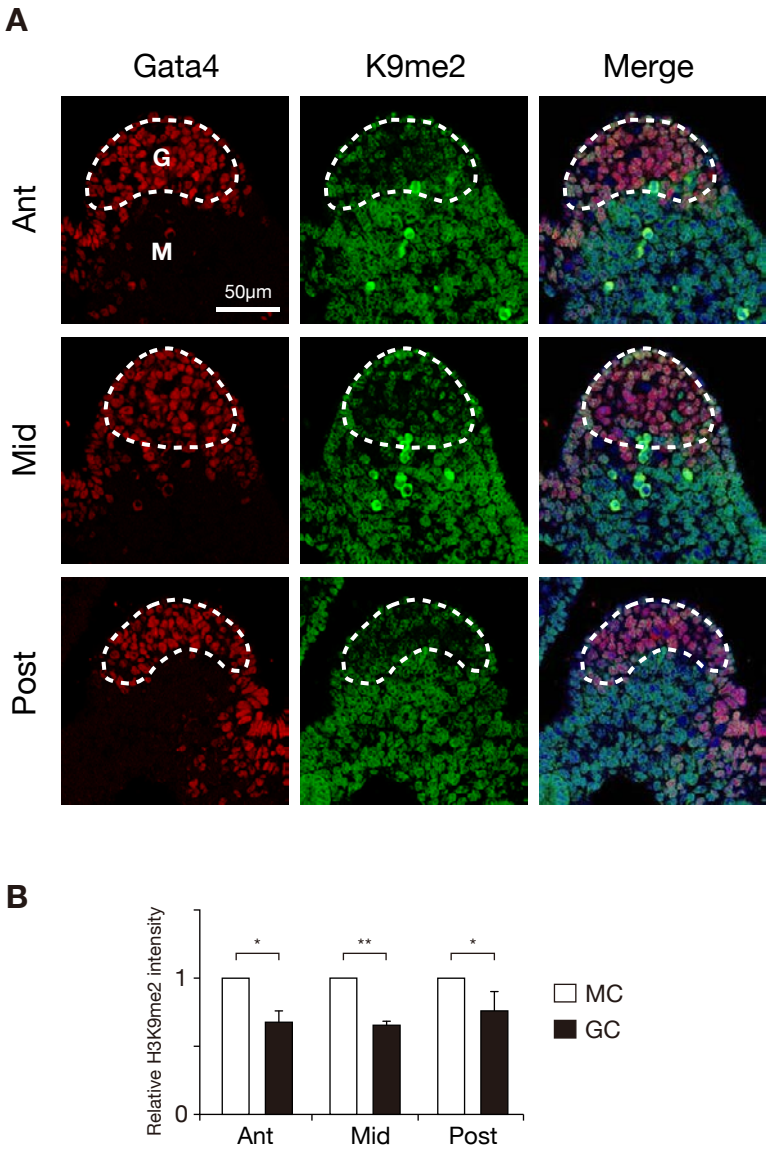

Fig. S12. Spatial distrubution of H3K9me2 in XY^{CBA} developng gonads.

(**A**) Co-immunostaining profiles of H3K9me2/Gata4 on sections of XY^{CBA} wild type gonads at 12ts. G, gonad; M, mesonephros; Ant, Anterior region; Mid, Middle region; Post, Posterior region. (**B**) Quantitative comparison of the immunofluorescence intensities of H3K9me2 signals between gonadal and mesonephric cells. Intensities of H3K9me2 signals of mesonephric cells were defined as 1. Data are presented as mean+s.e. *P<0.05, **P<0.01 (Student's t-test).

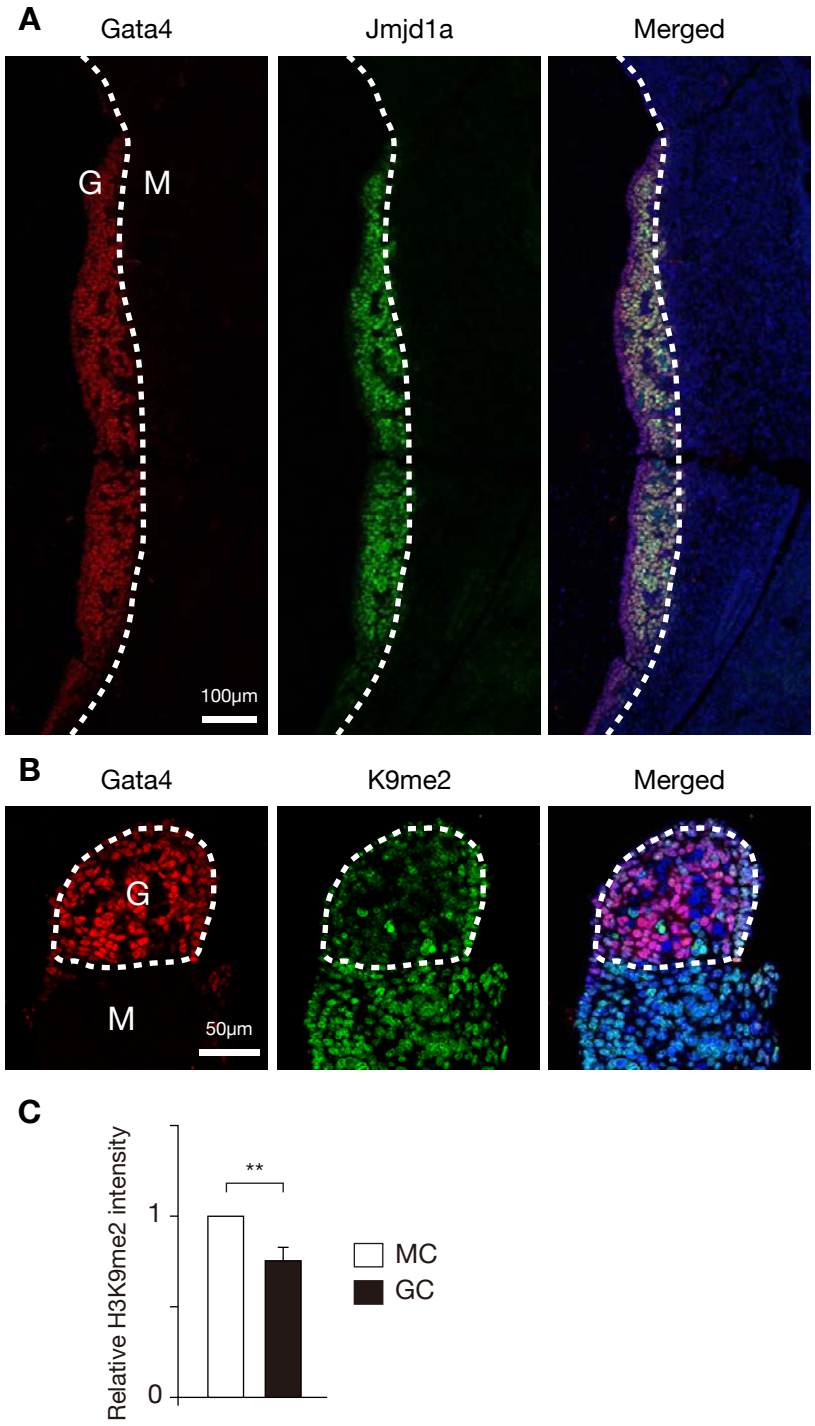

Fig. S13. Immunostaining profiles of Jmjd1a and H3K9me2 in developing female gonads.

XX wild type gonads at 18ts were immunostained with Jmjd1a/Gata4 (**A**) and H3K9me2/Gata4 (**B**). G, gonad; M, mesonephros. (**C**) Qunatitative copmparison of the immnunofluorescence intennsities of H3K9me2 signals between gonadal and mesonephric cells. Intensities of H3K9me2 signals of mesonephric cells were defined as 1. MC, mesonephric cells; GC, gonadal cells. Data are presented as mean±s.e. $^{**}P<0.01$ (Student's t-test).

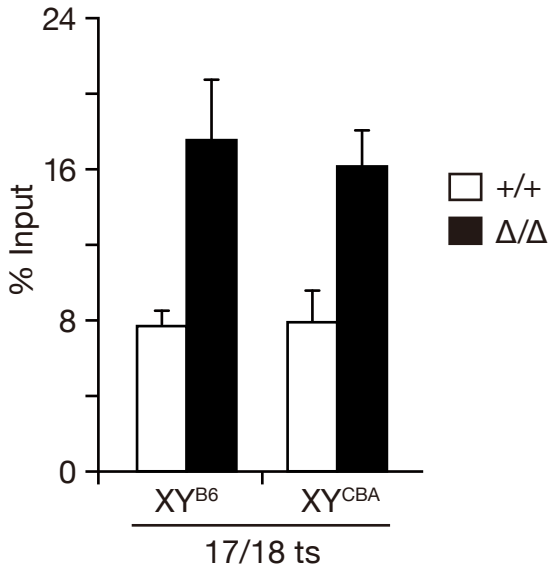

Fig. S14. Comparison of H3K9me2 levels of *Sry* loci between genetic background.
H3K9me2 levels of the *Sry* linear promoter region of E11.5 gonadal somatic cells of XY^{CBA} or XY^{B6} of indicated genotypes were determined by ChIP analysis. Data are presented as means±s.e.

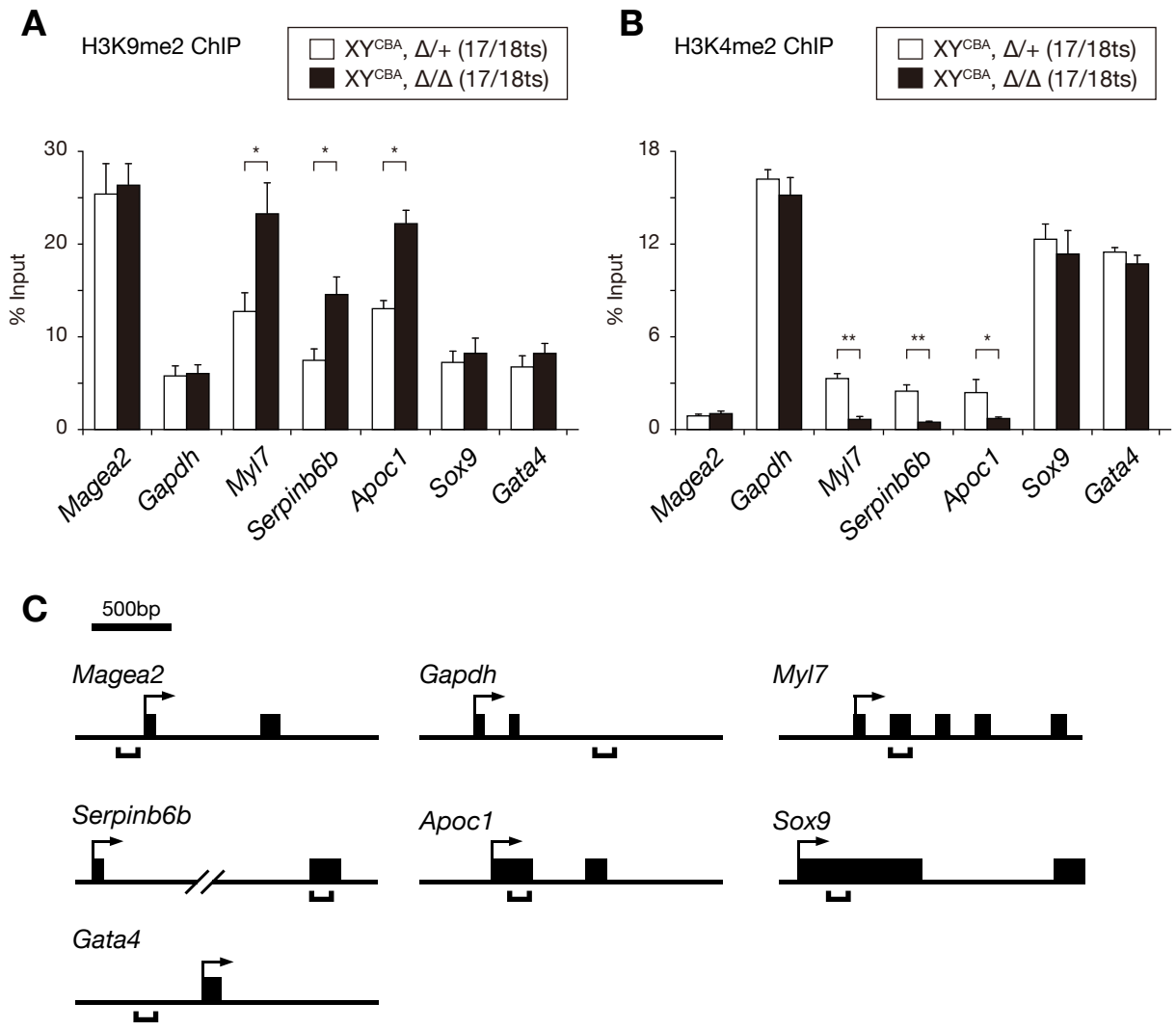

Fig. S15. Histone methylation status of Jmjd1a-target genes and control genes in gonadal somatic cells at E11.5.

The levels of H3K9me2 (**A**) and H3K4me2 (**B**) of the indicated loci were determined by ChIP analysis. (**C**) Diagram of the locus examined and the location of primer sets for ChIP-qPCR. *Myl7*, *Serpinb6b* and *Apoc1* were Jmjd1a-target genes identified by microarray analysis (Table S3). *Magea2* is a control locus abundant in H3K9me2. Data are presented as mean+s.e. **P*<0.05, ***P*<0.01 (Student's *t*-test).

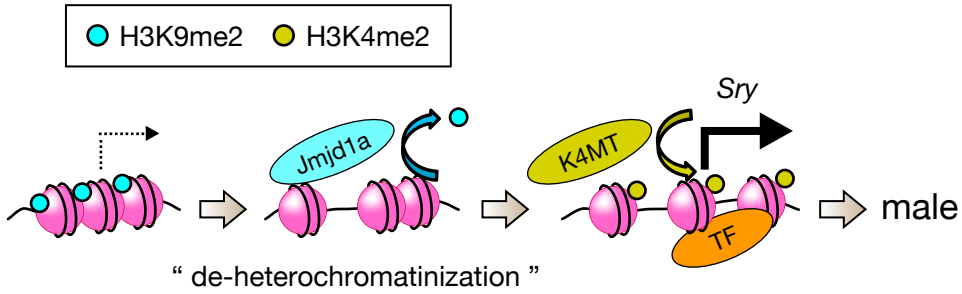

Fig. S16. Functions of Jmjd1a in mammalian sex determination.

K4MT, H3K4 methyltransferase. TF, transcription factor.

Table S1. Sex reversal of external genitalia and gonads in XY^{CBA} *Jmjd1a*-deficient mice

		External genitalia			Gonads			
		Male	intersex	female	testes	testis+ovary	ovaries	others
XY	+/+	54	0	0	54	0	0	0
	Δ/+	104	0	0	104	0	0	0
	Δ/Δ	11*	14§	33†#	7	12	34	5‡
XX	+/+	0	0	67	0	0	67	0
	Δ/+	0	0	153	0	0	153	0
	Δ/Δ	0	0	53¶	0	0	53	0

Chromosomal sex was determined by PCR analyses using primer sets for Y-chomoseome genes, *Sry*, *Zfy* and *Rbmy1a1*. Sex of external genitalia and gonads were defined as follows: a mouse with a penis was defined as male; a mouse with both penis-like external genitalia and incomplete vaginal orifice was defined as intersex; a mouse with vaginal orifice was defined as female.

*Of eleven animals, seven contained testes, three contained a testis and an ovary, and one contained an ovary and indistinct gonad.

§Of fourteen animals, nine contained a testis and an ovary, four contained only an ovary, and one contained ovaries.

†All animals contained ovaries.

‡Of five animals, four contained only an ovary. One contained an ovary and indistinct gonad.

#27 animals were naturally mated with fertile wild-type males. Among them, 11 animals exhibited fertilities.

¶ All animals were fertile.

Table S2. Reproductive activities of XY^{CBA} *Jmjd1a* Δ/Δ sex-reversed fertile animals

Fertile mice vaginally delivered pups		
Mice	Delivery times	Numbers of pups/delivery
#1	2	2, 2
#2	1	2
#3	1	1
#4	1	1

Fertile mice validated by cesarean section			
		Numbers of embryos	
Mice	Embryonic days	living	Postimplantation loss
#5	E10	4	2
#6	E12	1	1
#7	E13	1	1
#8	E14	3	1
#9	E16	1	1
#10	E18	3	0
#11	E18	2	1

Additiional Supplementary Data Table S3 (separate Excel file):

Table S3. List of the genes that affected by *Jmjd1a* deficiency in E11.5 gonadal somatic cells.

RNAs were collected from immunomagnetically purified gonadal somatic cells from a pair of gonads at 18ts. Examined samples were as follows: XY^{CBA} *Jmjd1a* Δ/+ (n=3), XY^{CBA} *Jmjd1a* Δ/Δ (n=3), XX *Jmjd1a* Δ/+ (n=3) and XX *Jmjd1a* Δ/Δ (n=3). Signal intensity data were analyzed with GeneSpring GX12 (Agilent Technologies). Genes down-regulated by *Jmjd1a* deficiency (< 0.5-fold, except for *Sox9*) or up-regulated by *Jmjd1a* deficiency (> 2.0-fold) were extracted (P<0.05). Genes regulated by Jmjd1a in XY gonads as well as XX gonads are shown in red.

Table S4. Primer list

Primer name	Application	Sequence (5'→3')
Gapdh RT-PCR F	RT-qPCR	ATGAATACGGCTACAGCAACAGG
Gapdh RT-PCR R	RT-qPCR	CTCTTGCTCAGTGTCCTTGCTG
Sry-5-SD	RT-qPCR	TACCTACTTACTAACAGCTGACATCAC
Sry-3-SD	RT-qPCR	TGTCATGAGACTGCCAACCACAGGG
Sox9-F	RT-qPCR	AGGAAGCTGGCAGACCAGTA
Sox9-R	RT-qPCR	CGTTCTTCACCGACTTCCTC
Wt1-e1-F	RT-qPCR	ATGGCCACACGCCCTCGCATCACGC
Wt1-e1-R	RT-qPCR	AGCGAGCCCTGCTGGCCCATGGGGT
Gata4-e1-F	RT-qPCR	GGGTAGGCCTCTCCTGTGCCAACTG
Gata4-e1-R	RT-qPCR	GAGGCCGCAGGCATTACATACAGGC
Wnt4-F	RT-qPCR	CCTGCGACTCCTCGTCTTC
Wnt4-R	RT-qPCR	AAGGTTCCGTTTGCACATCT
Jmjd1a exon 21F	RT-qPCR	ACTCCAGAGGATCGGAAATATGGGACC
Jmjd1a exon 21R	RT-qPCR	GGGAATTCCCACATAAACCATGACATTGGC
G9a-RT-1B	RT-qPCR	ACCCCAACATCATCCCTGTCCGGG
G9a-RT-2	RT-qPCR	GTCCCAGAATCGGTCACCGTAGTC
GLP-RT-1B	RT-qPCR	AACCCAACCTTGTGCCTGTGCGAG
GLP-RT-2	RT-qPCR	CGAGCTGCTCCCCAGCCTGAATCAG
Eset RT-PCR exon 15F	RT-qPCR	GCTGCTTGGATGATATTGCC
Eset RT-PCR exon 16R	RT-qPCR	CAGGCCTTCTTTGTCTGCAA
Suv39h1-F	RT-qPCR	CCATCTACGAGTGCAACTCCCGCTG
Suv39h1-R	RT-qPCR	AGATGCAGAGATCGTAGCGGATGCC
Suv39h2-F	RT-qPCR	TGACTTGGAGGGCCCACCTTTAGAC
Suv39h2-R	RT-qPCR	CTTCACTGTTTATGCTGATCCCGGG
Jmjd1b 62315F	RT-qPCR	GGAGATGCTGATGAGGTGACCAAGC
Jmjd1b 62415R	RT-qPCR	GGATCTTCTCTGCATCCTTCGCTGC
Jmjd1c exon 26F-2	RT-qPCR	TATGGGGTGAGAGCCTGCACTCTGA
Jmjd1c exon 26R	RT-qPCR	GTACCTGGTGAAGTGTTCCTGCTGGC
Jhdm1d-F	RT-qPCR	CGGAGAAAGATGAGGAAACTTCGAG
Jhdm1d-R	RT-qPCR	TTTGAGGACTTCCCTTGTATGGAGC
Phf2-F	RT-qPCR	ATTGTGAAGA AACTATCGTG GGTGG
Phf2-R	RT-qPCR	ACAGATCAGG CAGTACTTGGTCACC
PHF8-F	RT-qPCR	CAGAAGTACTGCCTCATGAGTGTGC
PHF8-R	RT-qPCR	GCACATGGTACCAAACTGAGGTCCC

Primer name	Application	Sequence (5'→3')
Sry distal-f	ChIP-qPCR	AACGCAAAGGTTGTTTCATTC
Sry distal-r	ChIP-qPCR	GAATCCCCTGAGTGCACATT
Sry circular prom.-f	ChIP-qPCR	GTGTAGGGGGATGGCATCTA
Sry circular prom.-r	ChIP-qPCR	TTCTCCAGAATGTTCACTCGAC
Sry linear prom.-f	ChIP-qPCR	TGGTCAGTGGCTTTTAGCTCT
Sry linear prom.-r	ChIP-qPCR	AGATGTGATGCAAAGAGAAACA
Sry 3'UTR-f	ChIP-qPCR	AGCTGACATCACTGGTGAGC
Sry 3'UTR-r	ChIP-qPCR	TCATAGCAAGGGGGAGTGTT
Gata4 prom.-f	ChIP-qPCR	GAGCTCACTTCAAGGGCCCCGTAGA
Gata4 prom.-r	ChIP-qPCR	AAGGTGACCTCGCACACTGGGCTCA
Magea2-90F	ChIP-qPCR	CGGAACCTCTGTGCTGACCTGTGGT
Magea2-2B	ChIP-qPCR	CGCTCCAGAACAAAATGGCGCAGA
Gapdh ChIP F	ChIP-qPCR	ATCCTGTAGGCCAGGTGATG
Gapdh ChIP R	ChIP-qPCR	AGGCTCAAGGGCTTTTAAGG
Myl7-e1-F	ChIP-qPCR	GGAAGGCTGG GACCCGAGGCAAGGC
Myl7-e1-R	ChIP-qPCR	AATTCCTGAATCTGGGCTTGTTCGA
Serpinb6b-ex2-F	ChIP-qPCR	GATCCACTGCTGGAAGCAAATGCCA
Serpinb6b-ex2-R	ChIP-qPCR	AGGTGAGAAAAGTACATTTCTGGAG
Apoc1-e1-F	ChIP-qPCR	CTGCCTCCAGGGTGCCCCTCCAACC
Apoc1-e1-R	ChIP-qPCR	AGGTCATGGCTACGACCACAATCAG
Sox-9-tss-300-F	ChIP-qPCR	CTGAGGGAAGAGGAGCCCCAGCCGC
Sox-9-tss-300-R	ChIP-qPCR	TCATGAAGGGGTCCAGGAGATTCAT

References

20. D. Wilhelm *et al.*, *Dev. Biol.* **287**, 111 (2005).
21. H. Kimura, Y. Hayashi-Takanaka, Y. Goto, N. Takizawa, N. Nozaki, *Cell Struct. Funct.* **33**, 61 (2008).
22. M. Tachibana, Y. Matsumura, M. Fukuda, H. Kimura, Y. Shinkai, *EMBO J.* **27**, 2681 (2008).
23. T. Yagi *et al.*, *Analytical biochemistry* **214**, 70 (1993).